INSTITUT D'AERONOMIE SPATIALE DE BELGIQUE

3 - Avenue Circulaire
B - 1180 BRUXELLES

AERONOMICA ACTA

A - N° 217 - 1980

Negative ion chemistry in the terrestrial D-region and signal flow graph theory

by

J. WISEMBERG and G. KOCKARTS

BELGISCH INSTITUUT VOOR RUIMTE-AERONOMIE

3 - Ringlaan
B - 1180 BRUSSEL

FOREWORD

The paper "Negative ion chemistry in the terrestrial D-region and signal flow graph theory" is accepted for publication in Journal of Geophysical Research, 85, 1980.

AVANT-PROPOS

L'article "Negative ion chemistry in the terrestrial D-region and signal flow graph theory" sera publié dans Journal of Geophysical Research, 85, 1980.

VOORWOORD

Het artikel "Negative ion chemistry in the terrestrial D-region and signal flow graph theory" zal verschijnen in Journal of Geophysical Research, 85, 1980.

VORWORT

Die Arbeit "Negative ion chemistry in the terrestrial D-region and signal flow graph theory" wird in Journal of Geophysical Research, 85, 1980 herausgegeben werden.

NEGATIVE ION CHEMISTRY IN THE TERRESTRIAL D-REGION AND SIGNAL FLOW GRAPH THEORY

by

J. WISEMBERG and G. KOCKARTS

Abstract

Aeronomic systems such as the negative ion chemistry in the D region are characterized by numerous reactions involving positive, negative and neutral species. Classical solutions of such system do not necessarily point out the role played by each parameter. When the chemical system is considered as a graph, it is possible to apply the signal flow graph technique which allows a quantitative evaluation of the various paths and loops. A negative ion model is obtained for daytime conditions by using the signal flow graph technique which is briefly described. This reference model is analyzed in terms of transmittances, path gains and loop gains. An arbitrary variation of atomic oxygen and nitric oxide is introduced at a height of 65 km in order to show the induced effects on the negative ions and, on the electron concentrations. Variations of the ratio λ between negative ions and electrons are also presented.

Résumé

Les systèmes aéronomiques tels que la chimie des ions négatifs dans la région D sont caractérisés par de nombreuses réactions impliquant des espèces positives, négatives et neutres. Les solutions classiques d'un tel système ne mettent pas nécessairement en évidence le rôle joué par chaque paramètre. Lorsque le système chimique est considéré comme un graphe, il est possible d'appliquer la technique des graphes de transfert qui permet une évaluation quantitative des différents chemins et circuits. Un modèle diurne d'ions négatifs est obtenu en utilisant la technique des graphes de transfert qui est brièvement décrite. Ce modèle de référence est analysé en termes de transmittances, de gains de chemin et de gains de circuits. Une variation arbitraire de l'oxygène atomique et de l'oxyde d'azote est introduite à 65 km d'altitude afin d'indiquer les effets induits sur la concentration des ions négatifs et des électrons. Les variations du rapport λ entre les ions négatifs et les électrons sont également présentées.

Samenvatting

Aëronomische systemen zoals de scheikunde van negatieve ionen in het D-gebied zijn gekenmerkt door talrijke reakties die betrekking hebben op positieve, negatieve en neutrale komponenten.

De gewonen oplossingen van zulk een systeem laten het niet noodzakelijk toe de rol gespeeld door iedere parameter aan het licht te komen.

Wanneer een chemisch systeem beschouwd wordt als een graph, dan is het mogelijk de graph overdrachttechniek toe te passen die de kwantitieve schatting toelaat van de verschillende beschouwde wegen en kringen.

Een negatief ion-model wordt bekomen voor dagvoorwaarden met behulp van de graph overdrachttechniek die bondig beschreven wordt. Dit referentiemodel wordt behandeld in termen van transmitantie, winst bij afgelegde wegen en beschouwde kringen. Een willekeurige verandering van atomisch zuurstof en stikstofoxyde wordt ingevoerd bij 65 km hoogte om de afgeleidde effekten op de concentratie der negatieve ionen en de elektronen aan te duiden. Veranderingen van de λ-verhouding tussen negatieve ionen en elektronen worden eveneens besproken.

Zusammenfassung

Aeronomische Systemen sowie die Chemie der negativen Ionen der D-Schihte sind durch haüfigen Reaktionen zwischen positiven, negativen und ungeladenen Teilchen characterisiert. Klassische Lösungen beschauen nicht unfehlbar die Rolle jedes Parameters. Wenn das chemische System wie ein Graph berücksichtigt wird ist es möglich die "Signal Flow Graph" Technik zu benutzen um eine Berechnung der verschiedenen Wegen and Kreisen festzustellen. Ein tägliches Model der negativen Ionen wird berechnet und die Technik ist kurz beschrieben. Dieses Referenzmodel wird mit Durchlässigkeiten, mit Wegen- und Kreisen- Verstärkungsfaktoren analysiert. Eine freie Variation in Sauerstoff und in Stickstoffoxide wird auf 65 km Höhe eingeführt um die Effekten auf den negativen Ionen- und Elektronendichten anzuzeigen. Variationen des Verhältnis λ zwischen negativen Ionen und Elektronen werden auch vorgestellt.

1. INTRODUCTION

Mass spectrometer observations (e.g., Narcisi and Bailey, 1965; Narcisi, 1967; Goldberg and Blumle, 1970; Narcisi et al., 1971; Arnold et al., 1971; Goldberg and Aikin, 1971; Narcisi et al., 1972; Johannessen and Krankowsky, 1972; Zbinden et al., 1973, 1975) have shown that the terrestrial D region is characterized by many positive and negative ions which result from external ionization processes leading initially to electrons, molecular oxygen, nitrogen, and nitric oxide positive ions. Heavy negative ions (Arnold and Henschen, 1978) as well as positive ions (Arijs et al., 1978; Arnold et al., 1978) have also been detected in the stratosphere with balloon-borne mass spectrometers.

Prior to any direct determination of negative ions in the D region, Reid (1964) showed that it is unlikely for O_2^- to be the dominant negative ion although its formation is rather easy by electron attachment to atmospheric molecular oxygen. This ion is actually an initial step in a long chain of reactions which has been investigated in recent years for understanding of negative ion chemistry in the terrestrial atmosphere (e.g., Turco and Sechrist, 1972a,b; Thomas et al., 1973a,b; Thomas, 1974; Turco, 1974; Ferguson, 1974; Reid, 1976; Swider, 1977). Approximately 60 chemical reactions are at present time involved in the negative ion chemistry of the D-region and this number does not account for possible negative clusters formation. A similar situation occurs for the positive ions leading to a total of the order of 120 chemical reactions. Comparisons between various theoretical models is not always easy since they usually differ not only by the adopted reaction scheme and the corresponding reaction rates but also by the model of the neutral minor constituents involved in various production and loss processes. When the neutral model and some poorly known reaction rates are considered as variable parameters, it appears that

the ion chemistry of the D-region readily becomes a "black box" from which it is difficult to extract quantitative informations regarding a specific parameter. In a system with a few reactions, a knowledge of the reaction rates and the neutral concentrations leads rather easily to a determination of the most important mechanisms. But, in large systems cycling processes and feedback mechanisms make such an analysis more difficult.

The purpose of the present paper is to introduce a new way for analyzing D-region ion chemistry by considering the large chemical system as a signal flow graph. Such a technique summarized in Appendix A gives a direct access to the "black box" by assigning quantitative values to any path or loop in the system and by showing quantitatively how any input to the system is transmitted along the various paths. Comparisons with in situ measurements are left out for future work.

A daytime neutral model atmosphere as well as ion reaction rates and electron ion-pair production rates are presented in section 2. The signal flow graph technique is then applied to the negative ion chemistry in section 3 which also contains a discussion of some computational problems associated with the steady-state solution. An oversimplified example is given in Appendix B in order to clarify the signal flow graph technique and to show the identity with a classical solution which is, however, unable to give the same amount of physical informations on the whole system. A reference model for the negative ions is presented in section 4 in terms of electron and ion concentrations, production and loss rate. The importance of various reaction paths is discussed as a function of height. Using the reference model a parametric analysis is made at 65 km altitude in section 5. Such an analysis indicates how variations of the neutral model can lead to different negative ion concentrations without any change of the adopted reaction rates. The potential contribution of signal flow graph technique is finally summarized in the last section.

2. RATE COEFFICIENTS, NEUTRAL MODEL AND ELECTRON ION-PAIR PRODUCTION

When electrons are produced in the D-region between the stratopause and the mesopause, a negative ion chemistry chain is initiated by attachment with major atmospheric neutral constituents and with ozone according to the following processes

$$e + O_2 + O_2 \rightarrow O_2^- + O_2 \; ; \; k_1 = 4 \times 10^{-30} \exp(-193/T) \quad (1)$$

$$e + O_2 + N_2 \rightarrow O_2^- + N_2 \; ; \; k_2 = 1 \times 10^{-31} \quad (2)$$

$$e + O_3 \rightarrow O^- + O_2 \; ; \; k_3 = 9.1 \times 10^{-12} (T/300)^{1.46} \quad (3)$$

where the reaction rate k_1 in $cm^6 s^{-1}$ is measured as a function of the temperature T by Truby (1972), k_2 in $cm^6 s^{-1}$ is given by Phelps (1969) and k_3 in $cm^3 s^{-1}$ is measured by Stelman et al. (1972). A schematic diagram of negative ion reactions based on Ferguson's (1974) analysis is given in Figure 1. The diagram includes photodestruction processes with coefficients J_i in s^{-1} since emphasis will be given to daytime negative chemistry. The neutral reactants, M being the total concentration, are indicated on each edge joining two negative ions. The hydration effects on the negative ions is neglected in Figure 1 (Ferguson, 1974) although Keesee et al. (1979) conclude that hydrates of CO_3^-, HCO_3^- and NO_3^- should be prevalent in the nighttime lower ionosphere which is not considered in the present paper. The reaction rate coefficients corresponding to Figure 1 are given in Table 1 which only contains measured values compiled by Albritton (1978). These rate constants correspond to a temperature of the order of 300 K and no

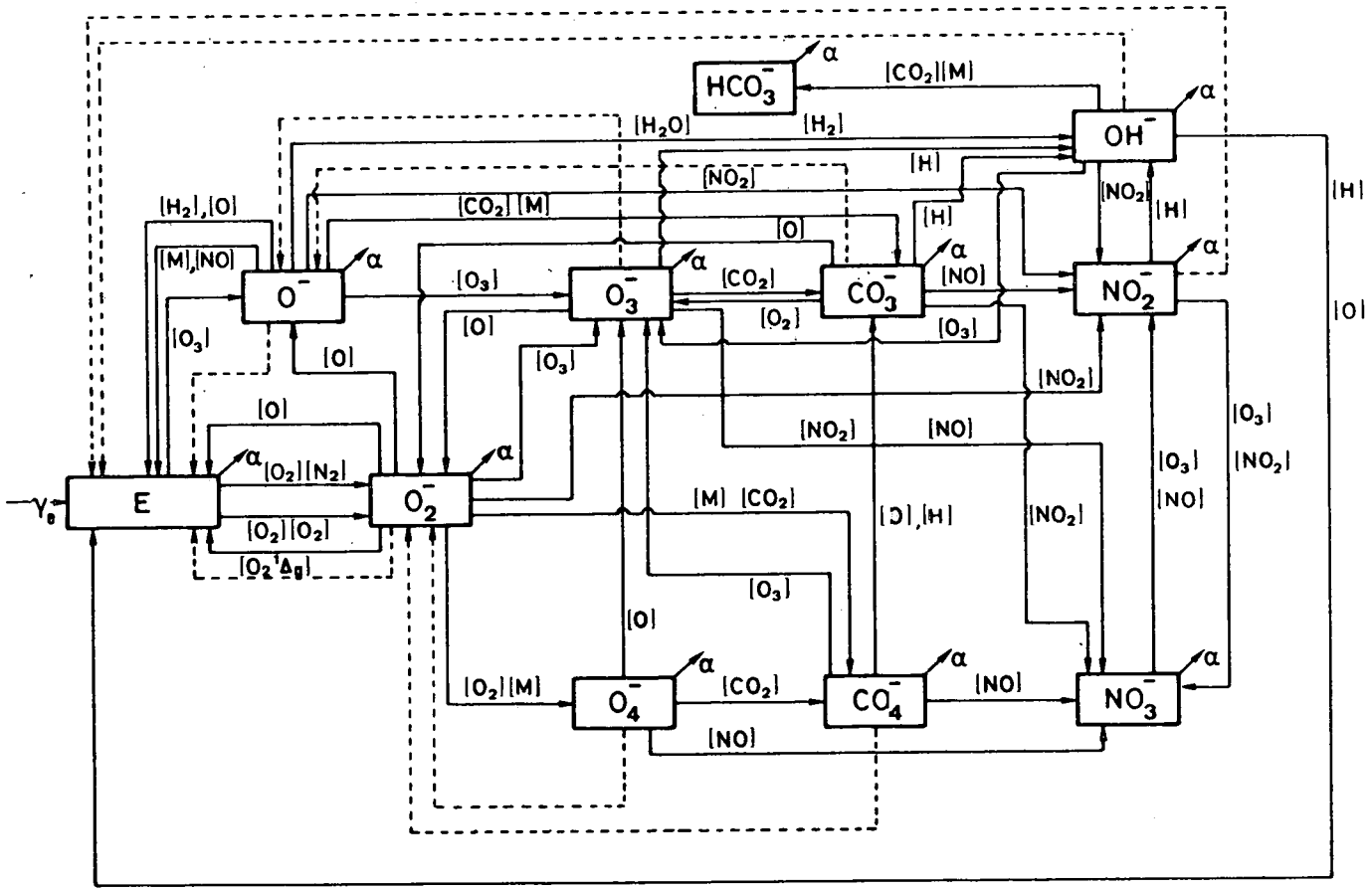

Fig. 1. Schematic diagram of negative ion reactions in the daytime D region. Neutral constituents involved in the reactions are indicated in brackets. Dashed lines correspond to photodestruction processes. Arrows labelled α correspond to dissociative recombination for electrons and to mutual neutralization for negative ions. The external production leading to electrons E and to positive ions is indicated by γ_e ($cm^{-3}s^{-1}$).

Table 1 : Negative ion reaction rates (Albritton, 1978) (two-body rates in $cm^3\ s^{-1}$; three-body rates in $cm^6\ s^{-1}$).

$O_2^- + O \rightarrow e + O_3$	1.5(-10)*
$O_2^- + O_2(^1\Delta_g) \rightarrow e + O_2 + O_2$	2.0(-10)
$O_2^- + CO_2 + M \rightarrow CO_4^- + M$	4.7(-29)
$O_2^- + O_3 \rightarrow O_3^- + O_2$	6.0(-10)
$O_2^- + NO_2 \rightarrow NO_2^- + O_2$	7.0(-10)
$O_2^- + O \rightarrow O^- + O_2$	1.5(-10)
$O_2^- + O_2 + M \rightarrow O_4^- + M$	3.4(-31)(1)
$O^- + O_2(^1\Delta_g) \rightarrow e + O_3$	3.0(-10)
$O^- + M \rightarrow e + \text{neutrals}$	1.0(-12)
$O^- + O_3 \rightarrow O_3^- + O$	8.0(-10)
$O^- + H_2 \rightarrow e + H_2O$	5.8(-10)
$O^- + H_2 \rightarrow OH^- + H$	6.0(-11)
$O^- + O \rightarrow e + O_2$	1.9(-10)
$O^- + NO \rightarrow e + NO_2$	2.1(-10)
$O^- + CO_2 + M \rightarrow CO_3^- + M$	2.0(-28)
$O^- + NO_2 \rightarrow NO_2^- + O$	1.0(-9)
$O^- + H_2O \rightarrow OH^- + OH$	6.0(-13)
$O_4^- + O \rightarrow O_3^- + O_2$	4.0(-10)
$O_4^- + NO \rightarrow NO_3^- + O_2$	2.5(-10)
$O_4^- + CO_2 \rightarrow CO_4^- + O_2$	4.3(-10)
$O_3^- + O \rightarrow O_2^- + O_2$	2.5(-10)
$O_3^- + NO \rightarrow NO_3^- + O$	2.6(-12)
$O_3^- + CO_2 \rightarrow CO_3^- + O_2$	5.5(-10)
$O_3^- + NO_2 \rightarrow NO_3^- + O_2$	2.8(-10)
$O_3^- + H \rightarrow OH^- + O_2$	8.4(-10)

Table 1 : (continued).

$CO_4^- + NO \rightarrow NO_3^- + CO_2$	4.8(-11)
$CO_4^- + O \rightarrow CO_3^- + O_2$	1.4(-10)
$CO_4^- + O_3 \rightarrow O_3^- + CO_2 + O_2$	1.3(-10)
$CO_4^- + H \rightarrow CO_3^- + OH$	2.2(-10)
$NO_3^- + O_3 \rightarrow NO_2^- + O_2 + O_2$	1.0(-13)
$NO_3^- + NO \rightarrow NO_2^- + NO_2$	1.0(-12)
$NO_2^- + H \rightarrow OH^- + NO$	3.0(-10)
$NO_2^- + O_3 \rightarrow NO_3^- + O_2$	1.2(-10)
$NO_2^- + NO_2 \rightarrow NO_3^- + NO$	2.0(-13)
$OH^- + H \rightarrow e + H_2O$	1.4(-9)
$OH^- + O_3 \rightarrow O_3^- + OH$	9.0(-10)
$OH^- + O \rightarrow e + HO_2$	2.0(-10)
$OH^- + NO_2 \rightarrow NO_2^- + OH$	1.1(-9)
$OH^- + CO_2 + O_2 \rightarrow HCO_3^- + O_2$	7.6(-28)
$CO_3^- + O \rightarrow O_2^- + CO_2$	1.1(-10)
$CO_3^- + NO_2 \rightarrow NO_3^- + CO_2$	2.0(-10)
$CO_3^- + NO \rightarrow NO_2^- + CO_2$	1.1(-11)
$CO_3^- + O_2 \rightarrow O_3^- + CO_2$	6.0(-15)
$CO_3^- + H \rightarrow OH^- + CO_2$	1.7(-10)

---

* 1.5(-10) corrresponds to 1.5×10^{-10}

(1) measured with M = He

attempt will be made here to introduce temperature dependences. Negative ions and electrons are also subjet to recombination with positive ions. For any negative ion X^- a recombination coefficient α_1 with any positive ion Y^+ is adopted from Smith et al. (1976) such that

$$X^- + Y^+ \rightarrow \text{neutrals} \qquad \alpha_1 = 6 \times 10^{-8} \text{ cm}^3 \text{ s}^{-1} \tag{4}$$

The dissociative recombination coefficients for O_2^+ and NO^+ are taken from Mul and McGowan (1979)

$$e + O_2^+ \rightarrow \text{neutrals} \qquad \alpha_2 = 1.9 \times 10^{-7} \, (300/T)^{0.5} \text{ cm}^3 \text{ s}^{-1} \tag{5}$$

and

$$e + NO^+ \rightarrow \text{neutrals} \qquad \alpha_3 = 2.3 \times 10^{-7} \, (300/T)^{0.5} \text{ cm}^3 \text{ s}^{-1} \tag{6}$$

The recombination rate coefficient of electrons with other positive ions such as clusters is adopted as

$$e + Y^+ \rightarrow \text{neutrals} \qquad \alpha_4 = 3 \times 10^{-6} \text{ cm}^3 \text{ s}^{-1} \tag{7}$$

in agreement with the values of Huang et al. (1978) for water cluster ions. Photodestruction cross sections have beem measured and summarized by Smith et al. (1978) and by Lee and Smith (1979). Using

these cross sections and the solar fluxes of Smith and Gottlieb (1974) the following photodetachment rates are obtained : $J_{O^-} = 1.4\ s^{-1}$, $J_{O_2^-} = 0.38\ s^{-1}$, $J_{OH^-} = 1.1\ s^{-1}$ and $J_{NO_2^-} = 8 \times 10^{-4}\ s^{-1}$. The photodissociation of CO_3^- leads to O^- and CO_2 with a rate $J_{CO_3^-} = 0.15\ s^{-1}$ whereas the photodissociation of O_3^- leads to O^- and O_2 with a rate $J_{O_3^-} = 0.47\ s^{-1}$. The photodissociation cross section of O_3^- is, however, characterized by a fine structure which requires further studies (Lee and Smith, 1979). Photodestruction of CO_4^- and O_4^- are assumed to give O_2^- with rates of $J_{CO^-} = 6.2 \times 10^{-3}\ s^{-1}$ and $J_{O^-} = 0.24\ s^{-1}$, although Cosby et al. (1976) are not excluding photodetachment. At present time the branching ratio between photodetachment and photodissociation is, however, not known. According to Cosby et al. (1976), HCO_3^- apparently neither photodetaches or photodissociates for wavelengths above 458 nm. Since the electron affinity of NO_3^- is 3.9 ± 0.2 eV. (Ferguson et al., 1972) no photodetachment mechanism for this ion is introduced in the present work. The negative ion system corresponds, therefore, to 44 ion neutral reactions given in Table 1, to three attachment processes given by Eqs (1) to (3) and to 8 photodestruction processes. The coupling between the negative ions and the positive ions occurs through reactions (4) to (6) which imply a knowledge of the positive ion concentrations.

Instead of fulfilling the condition of electroneutrality with a fictious positive ion Y^+, individual positive ions are computed with the measured reactions rates (Albritton, 1978; Ferguson, 1974) given in Table 2 without any temperature dependence. The sole significant photodissociation coefficient for positive clusters is computed for $O_2^+.H_2O$ with the cross sections of Smith and Lee (1978) and it leads to a value $J_{O_2^+.H_2O} = 0.42\ s^{-1}$. The introduction of a detailed positive ionic model is made to account for a possible simultaneous effect of certain parameters on the positive and negative ion chemistry. Such an effect could lead to a non linear coupling between positive and negative systems.

The neutral concentrations involved in Table 1 and in Table 2 are taken from the U.S. Standard Atmosphere (1976). for noon conditions at 45°N latitude. Such a model is similar to the recent mesospheric model developed by Keneshea et al. (1979). Since NO and NO_2 concentrations are not given in this model, we adopt the high daytime values computed by Turco and Sechrist (1970; 1972b). Vertical profiles of minor constituents used in our negative ionic reference model are summarized in Figure 2. Finally the electron ion pair productions used in the computations are shown in Figure 3. The quantities given in Figs. 2 and 3 are variable, but they are adopted here as reference values. The effect of possible variations of atomic oxygen and nitric oxide will described in section 5 as an application of the signal flow graph technique. This technique is presented in the following two sections for the negative ion model resulting from the reaction scheme, the electron ion-pair production and the neutral model just described.

3. SIGNAL FLOW GRAPH TECHNIQUE AND ION CHEMISTRY

The ionic scheme given in Figure 1 has all characteristics of a signal flow graph described in Appendix A. The various negative ionic species are nodes of the graph. Two consecutive nodes are joined by an edge indicating which neutral constituent is involved in the transformation and successive edges form a path which can become a loop when the initial and final negative ions are identical. The input γ_e to the system represents the electron ion-pair production. Under equilibrium conditions between k types of negative ions including electrons, Equation (B3) of Appendix B reduces to

$$P_i = T_{(i \leftarrow 1)} \times \gamma_e \qquad (8)$$

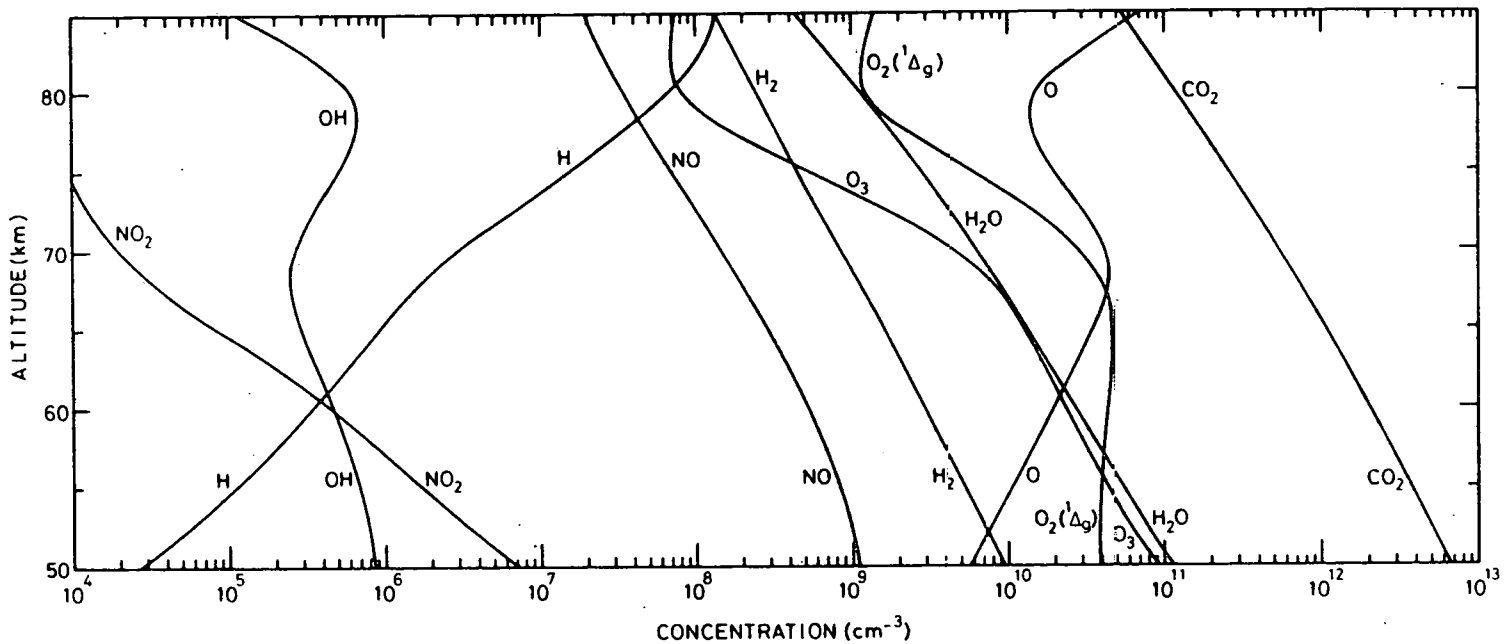

Fig. 2. Vertical profiles of neutral minor constituents involved in D-region ion chemistry. Noontime conditions at 45°N latitude.

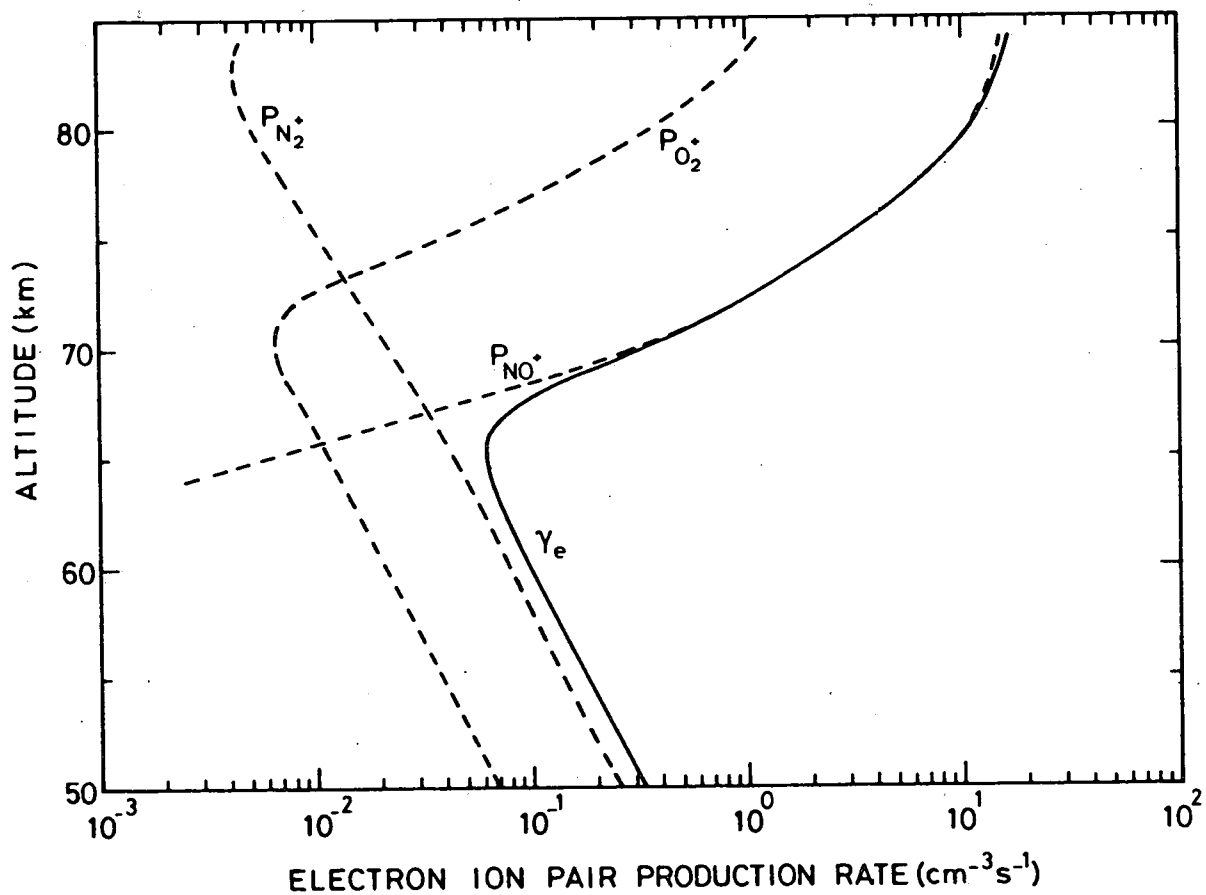

Fig. 3. Altitude dependence of the external electron production rate γ_e. Production rates of N_2^+, O_2^+ and NO^+ ions are also indicated.

Table 2 : Positive ion reaction rates (Albritton, 1978) (two-body rates in $cm^3 s^{-1}$; three-body rates in $cm^6 s^{-1}$).

$N_2^+ + O$	$\rightarrow NO^+ + N$	1.4(-10)*
$N_2^+ + O_2$	$\rightarrow O_2^+ + N_2$	4.3(-11)
$O_2^+ + N_2 + N_2$	$\rightarrow O_2^+.N_2 + N_2$	8.0(-31)
$O_2^+ + H_2O + N_2$	$\rightarrow O_2^+.H_2O + N_2$	2.8(-28)
$O_2^+ + H_2O + O_2$	$\rightarrow O_2^+.H_2O + O_2$	2.3(-28)
$O_2^+ + NO$	$\rightarrow NO^+ + O_2$	4.4(-10)
$O_2^+ + O_2 + O_2$	$\rightarrow O_4^+ + O_2$	2.5(-30)
$O_2^+.N_2 + H_2O$	$\rightarrow O_2^+.H_2O + N_2$	4.0(-9)
$O_2^+.N_2 + N_2$	$\rightarrow O_2^+ + N_2 + N_2$	2.0(-11)
$O_2^+.N_2 + O_2$	$\rightarrow O_4^+ + N_2$	5.0(-11)
$O_4^+ + H_2O$	$\rightarrow O_2^+.H_2O + O_2$	1.8(-9)
$O_4^+ + O$	$\rightarrow O_2^+ + O_3$	3.0(-10)
$O_4^+ + O_2$	$\rightarrow O_2^+ + O_2 + O_2$	1.8(-13)
$O_2^+.H_2O + H_2O$	$\rightarrow H_3O^+ + OH + O_2$	2.4(-10)
$O_2^+.H_2O + H_2O$	$\rightarrow H_3O^+.OH + O_2$	1.4(-9)
$H_3O^+ + H_2O + M$	$\rightarrow H_3O^+.H_2O + M$	7.0(-28)
$H_3O^+.OH + H_2O$	$\rightarrow H_3O^+.H_2O + OH$	2.0(-9)
$H_3O^+.H_2O + H_2O + M$	$\rightarrow H_3O^+.2H_2O + M$	2.0(-27)
$H_3O^+.2H_2O + H_2O + M$	$\rightarrow H_3O^+.3H_2O + M$	2.0(-27)
$H_3O^+.3H_2O + M$	$\rightarrow H_3O^+.2H_2O + H_2O + M$	4.0(-15)
$H_3O^+.3H_2O + H_2O + M$	$\rightarrow H_3O^+.4H_2O + M$	1.0(-29)
$H_3O^+.4H_2O + M$	$\rightarrow H_3O^+.3H_2O + H_2O + M$	4.0(-15)
$NO^+ + N_2 + N_2$	$\rightarrow NO^+.N_2 + N_2$	1.5(-30)
$NO^+ + H_2O + M$	$\rightarrow NO^+.H_2O + M$	1.3(-28)
$NO^+ + CO_2 + M$	$\rightarrow NO^+.CO_2 + M$	5.0(-29)
$NO^+.CO_2 + H_2O$	$\rightarrow NO^+.H_2O + CO_2$	1.0(-9)
$NO^+.H_2O + H$	$\rightarrow H_3O^+ + NO$	7.0(-12)

Table 2 : (continued)

$NO^+.H_2O + OH$	$\rightarrow H_3O^+ + NO_2$	1.0(-10)
$NO^+.H_2O + H_2O + M$	$\rightarrow NO^+.2H_2O + M$	9.0(-28)
$NO^+.2H_2O + H_2O + M$	$\rightarrow NO^+.3H_2O + M$	1.0(-27)
$NO^+.2H_2O + M$	$\rightarrow NO^+.H_2O + H_2O + M$	1.5(-14)
$NO^+.3H_2O + M$	$\rightarrow NO^+.2H_2O + H_2O + M$	1.0(-12)
$NO^+.3H_2O + H_2O$	$\rightarrow H_3O^+.2H_2O + HNO_2$	7.5(-11)
$NO^+.N_2 + CO_2$	$\rightarrow NO^+.CO_2 + N_2$	1.0(-9)(1)

* 1.4(-10) corresponds to 1.4×10^{-10}

(1) see Ferguson (1974)

where P_i is the production rate (cm^{-3} s^{-1}) of the i-type ion and $T_{(i \leftarrow 1)}$ is the transmittance given by

$$T_{(i \leftarrow 1)} = \sum g_\ell \Delta_\ell / \Delta \qquad (9)$$

In Equation (9), n is the number of paths leading from the sole input 1 to the i-type ion. The path gains g_ℓ and the amplification factors Δ_ℓ/Δ are given by Mason's (1956) rules described in Appendix A and applied to an oversimplified example in Appendix B. Computation of the production rates P_i by Equation (8) leads immediately to the concentrations n_i, since

$$n_i = P_i / L_i \qquad (10)$$

where L_i is the total loss rate (s^{-1}) of the i-type ion. It is shown in Appendix B that the total loss rates L_i are simultaneously computed with the path gains g_ℓ.

Mason's (1956) rules are strictly valid for linear systems of equations. Mutual neutralization between negative and positive ions as well as dissociative recombination between electron and positive ions can a priori introduce some non linearity since the positive ions are not necessarily known. Such a non linearity can be removed with help of the electroneutrality condition. Starting with two arbitrary relative distributions of n positive ions with relative concentration x_i^+ and m negative ions (including electrons) with relative concentration x_j^- such that

$$\Sigma \; x_i^+ = \sum_{j=1}^{m} x_j^- = 1 \qquad (11)$$

it is possible to calculate an effective recombination coefficient

$$\alpha_{eff} = \sum_{i=1}^{n} \sum_{j=1}^{m} \alpha_{ij} \, x_i^+ \, x_j^- \qquad (12)$$

where the recombination coefficients are given by Equations (4) to (7). The corresponding total positive or negative concentration n_t is then

$$n_t = (\gamma_e/\alpha_{eff})^{1/2} \qquad (13)$$

where γ_e is the input production rate. An initial set of positive and negative ions is obtained from the relations

$$n_i^+ = x_i^+ \times n_t \qquad (14)$$

and

$$n_j^- = x_j^- \times n_t \qquad (15)$$

The set of positive ions is used for a solution of the negative ion system and the resulting negative ions are used to compute a new set of relative distributions x_j^-. The same procedure is used for the

positive ions and the iteration scheme (11) to (15) is repeated untill convergence is reached. Convergence within one percent is obtained after three iterations.

Before solving the negative or positive ion system it is necessary to make a computer search of the various paths leading to a specific ion from the input γ_e. This can be done by associating a logical square matrix to the graph. The number of rows and columns of this matrix is equal to the number of nodes of the graph. An element (i, j) of this matrix is set to one if the i-th ion can lead to the j-th ion. In such a way any value one in the i-th row indicates that the ion associated with the corresponding j-th column can be produced by the i-th ion. All unitary values in the i-th row indicate the "descendants" of the i-th ion and all unitary value in the i-th column give the "ascendants" of the i-th ion. An analysis of each column leads then to the various paths which are memorized only if the last node is an input node and if a path does not go twice through a same node. Loops are obtained by considering each node as an input. Care must be taken to avoid multiple counting of loops resulting from input nodes which belong to the same loop. The total number of paths in Figure 1 is 729 and O_4^- is produced by 12 paths, O_2^- by 12 paths, CO_4^- by 24 paths, O^- by 28 paths, CO_3^- by 32 paths, O_3^- by 44 paths, OH^- by 112 paths, NO_2^- by 142 paths, HCO_3^- by 156 paths and NO_3^- by 167 paths, respectively. The absolute abundance of a specific ion is not correlated with the number of paths. Expression (8) shows that the ion concentration is actually proportional to the transmittance which depends on the path gains and the amplification factors.

The efficiency of the signal flow graph technique is particularly high for large systems where the great number of paths and loops makes it very difficult to find the most important mechanisms leading to a specific ion. In the numerical results of the next section we have neglected the paths which contribute by less than one percent to the transmittance from the input to each i-type ion.

4. ANALYSIS OF THE REFERENCE MODEL FOR NEGATIVE IONS

The signal flow graph technique can be applied at any height in the D-region as long as transport processes are negligible. The neutral model combined with the reaction rates and the electron production given in section 2 leads to the vertical profiles shown in Figure 4. Only the most important negative ions and the electron concentration are indicated. The dimensionless ratio λ between the total negative ion concentration and the electron concentration is given to show the height range where negative ions are more abundant than electrons. The ratio λ becomes equal to one near 69 km altitude. In the height range where negative ions are important, NO_3^- is always the most abundant ion although CO_3^- and HCO_3^- are not completely negligible. This result is in contradiction with the model of Thomas et al. (1973b), where photodetachment was introduced as an important process, but it is in better agreement with the calculations of Turco and Sechrist (1972a, b). Furthermore the presence of HCO_3^- in Figure 4 is a direct consequence of its small loss rate by mutual neutralization with positive ions. Such differences are a direct consequence of the different neutral models, the different reaction schemes and the different rate coefficients used in these ionic models. We will see in section 5 how variations in the neutral model modify the relative abundances of the major negative ions. At present time the results of Figure 4 are considered as a reference model for which we want to show the type of information gained by the signal flow graph technique.

The initial electron production results from the input γ_e given in Figure 3, but electrons can be subsequently produced from other negative ions by photodetachment and by ion-neutral reactions. The importance of this effect is shown in Figure 5 which shows the electron production resulting from several negative ions. Figure 5 indicates that the transmittances reach values much larger than one when electron

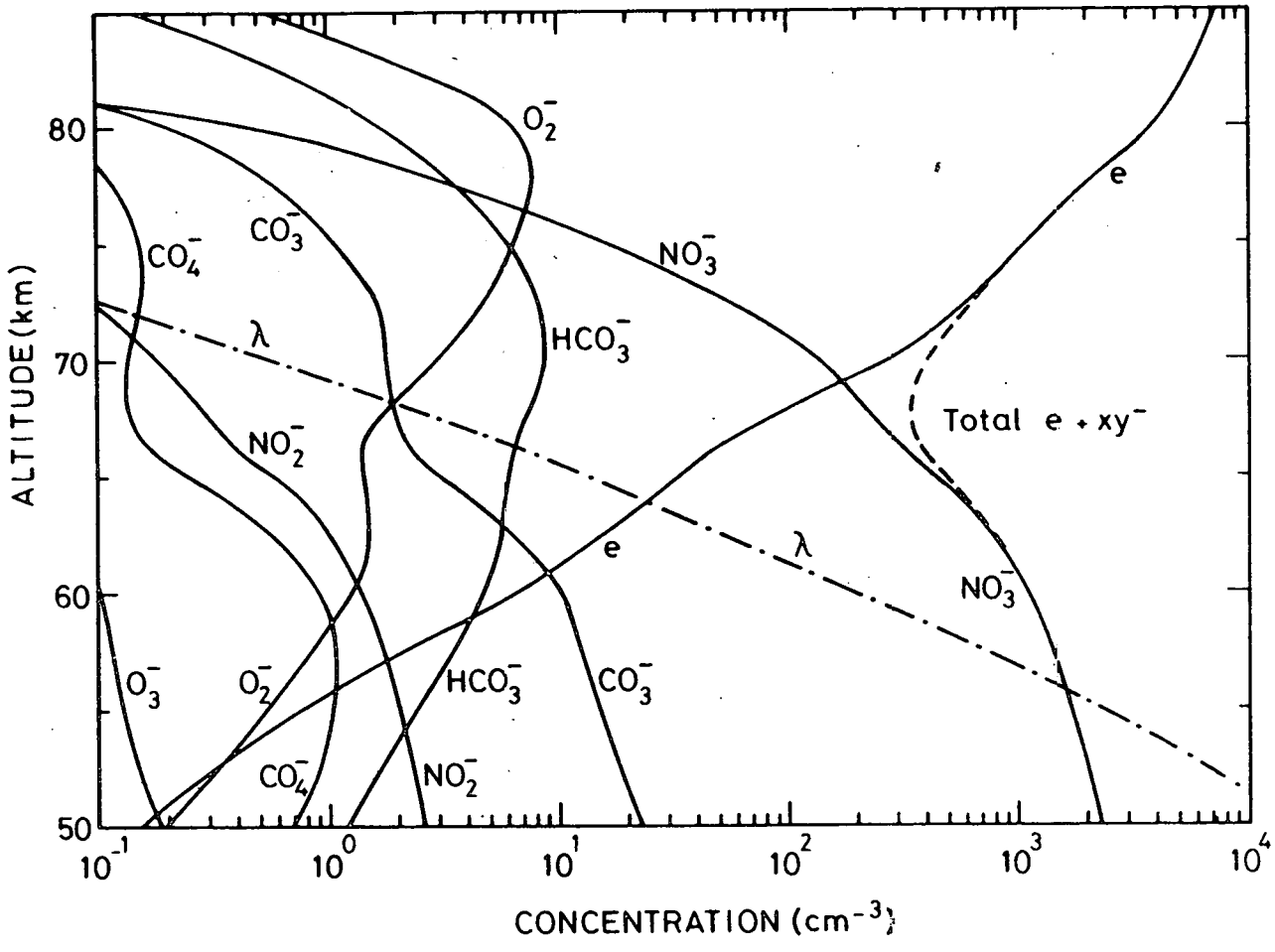

Fig. 4. Vertical profiles of negative ions and electrons. The ratio λ between the negative ion concentration and the electron concentration is given by the dotted-dashed lines whereas the sum of the electron and negative ion concentration is given by the dashed line.

productions resulting for a negative ion XY^- is greater than the input value γ_e. All curves or parts of curves to the righthand side of the input γ_e correspond to amplification by chemical and photochemical processes such that the transmittance in Equation (8) is greater than one. At all heights below 82 km the electron production resulting from the negative ions is larger than the direct input production. Above 55 km altitude, O_2^- leads to the major electron production rate, although O_2^- is never a major negative ion in the region where negative ion concentrations are comparable or greater than the electron concentration (see Figure 4). Figure 5 should not be interpreted as a mysterious electric charge creation resulting from the input γ_e since the electron loss rates are always such that the electroneutrality condition is satisfied.

Negative ion production rates are shown in Figure 6 for the input γ_e of Figure 3. The production rates of negative ions are always equal or greater than the electron production rates resulting from these ions, since mutual neutralization and photodissociation included in the transmittances leading to Figure 5 never lead to electron production. Furthermore, the losses of negative ions included in the transmittances leading to Figure 5, do not necessarily lead to electron production.

In our reference model, NO_3^- and CO_3^- and HCO_3^- are the major negative ions. The signal flow graph technique automatically allows a quantitative determination of the most important paths leading to these ions. Figure 7 shows the total production rates of NO_3^- and CO_3^- and the contribution of all paths leading at least to 1 percent of the total production. Each path is characterized by a number which is obtained following the technique described in section 3. and the various paths are identified in Table 3. It appears that a path can be almost negligible in a certain height range and can become very important in another height range. The partial productions resulting from a specific path are not represented anymore in Figure 7 when they contribute for

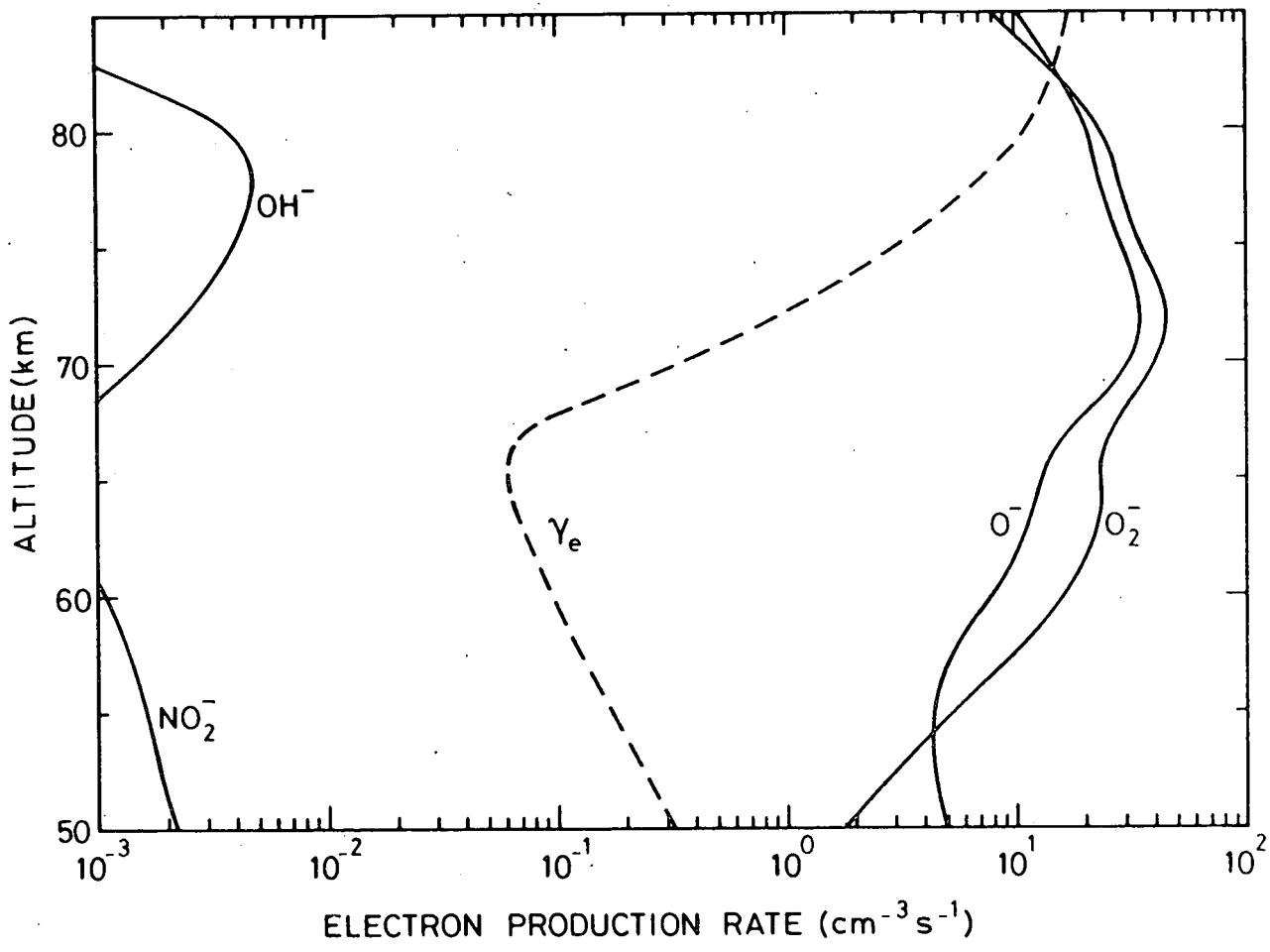

Fig. 5. Vertical distribution of the electron production rates resulting through photodetachment and collisional detachment of various negative ions. The dashed curve represents the external input γ_e of Fig. 3.

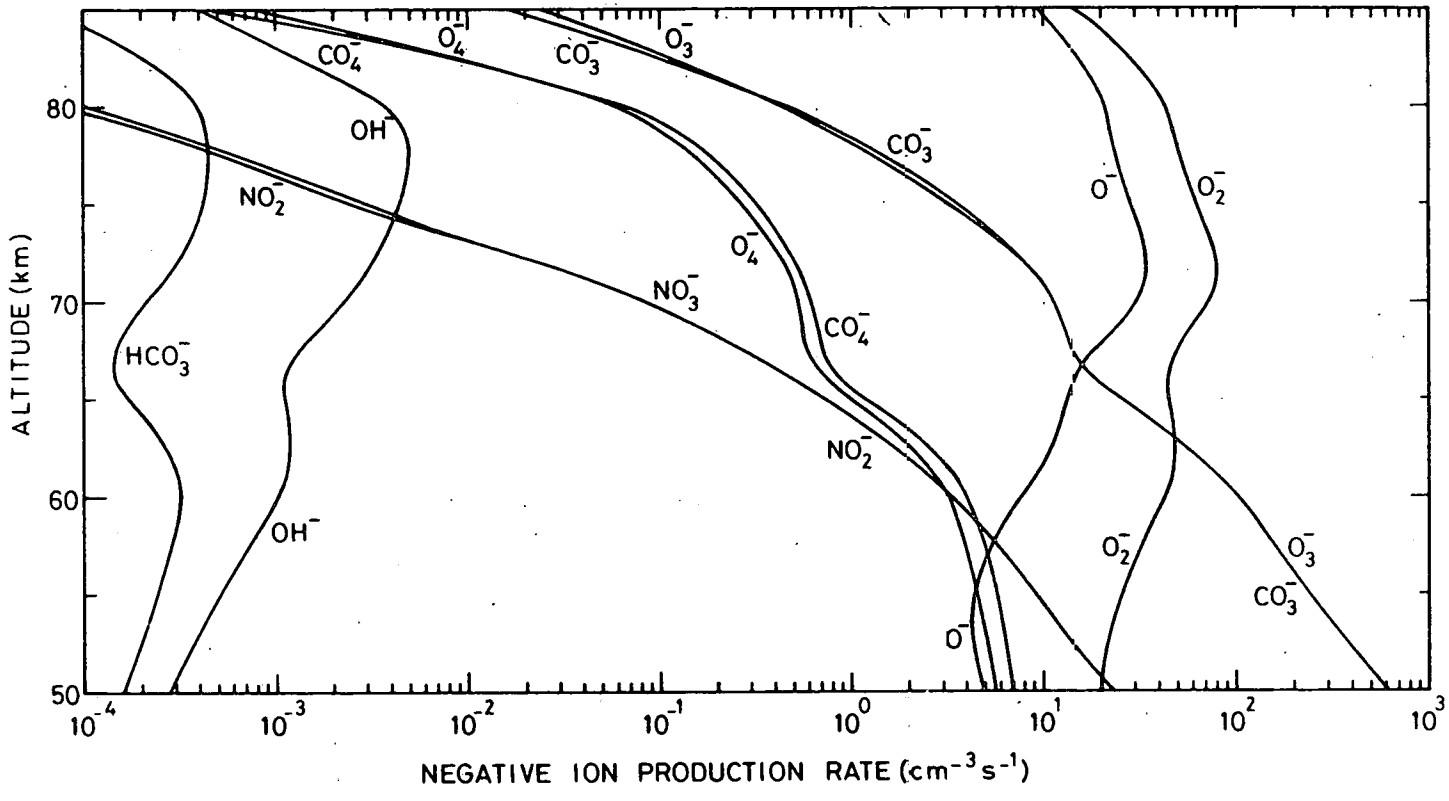

Fig. 6. Vertical distributions of various negative ion production rates for the external input γ_e of Fig. 3.

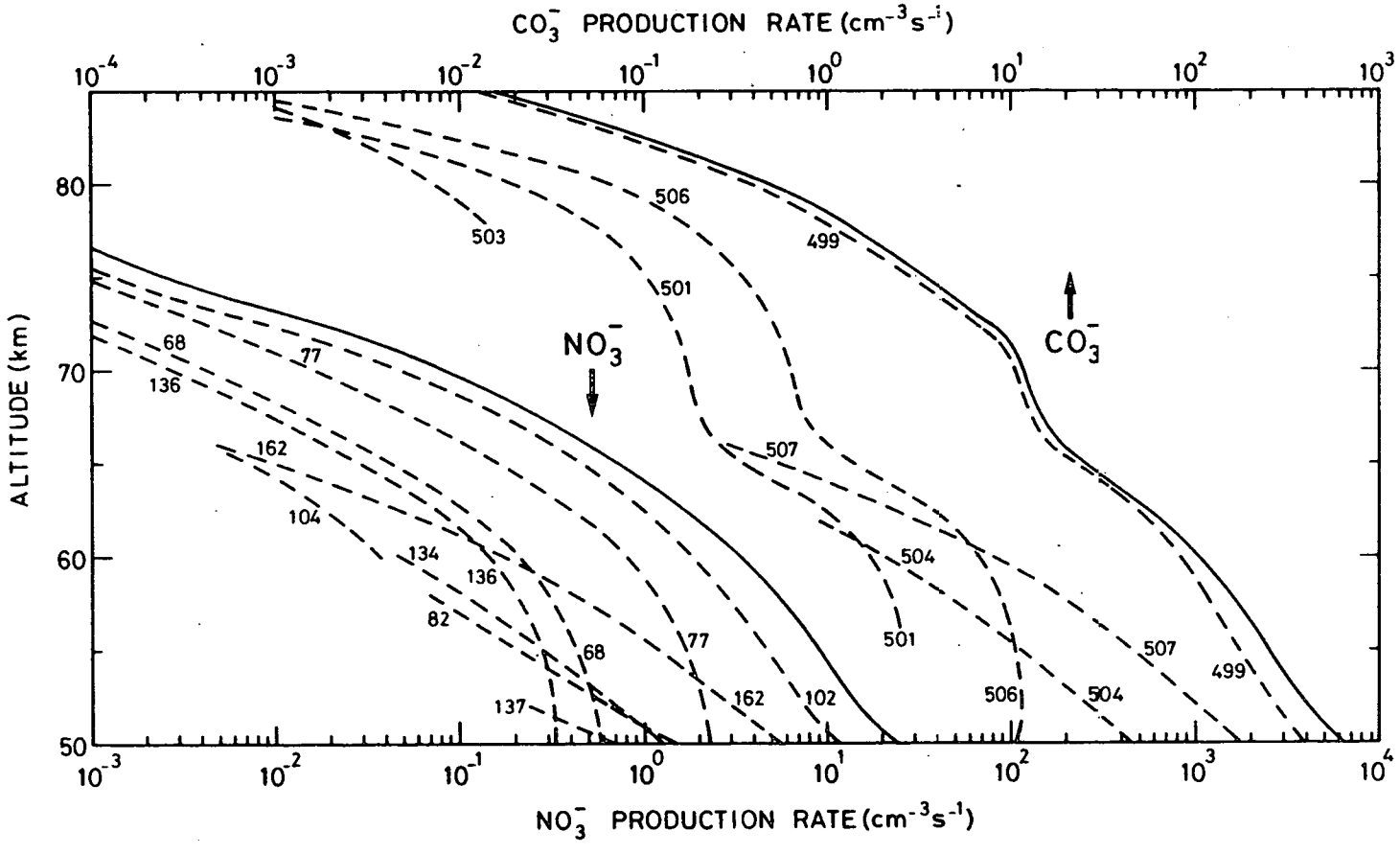

Fig. 7. Contribution of individual paths to NO_3^- and CO_3^- production rates. The paths are identified in Table 3.

Table 3 : Paths leading to NO_3^- and CO_3^- ions.

Path number	Path
68	$e \rightarrow O_2^- \rightarrow CO_4^- \rightarrow NO_3^-$
77	$e \rightarrow O_2^- \rightarrow O_4^- \rightarrow CO_4^- \rightarrow NO_3^-$
82	$e \rightarrow O_2^- \rightarrow O_3^- \rightarrow CO_3^- \rightarrow NO_3^-$
102	$e \rightarrow O_2^- \rightarrow O_3^- \rightarrow CO_3^- \rightarrow NO_2^- \rightarrow NO_3^-$
104	$e \rightarrow O_2^- \rightarrow CO_4^- \rightarrow CO_3^- \rightarrow NO_2^- \rightarrow NO_3^-$
134	$e \rightarrow O_2^- \rightarrow CO_4^- \rightarrow O_3^- \rightarrow CO_3^- \rightarrow NO_2^- \rightarrow NO_3^-$
136	$c \rightarrow O_2^- \rightarrow O_4^- \rightarrow CO_4^- \rightarrow CO_3^- \rightarrow NO_2^- \rightarrow NO_3^-$
137	$e \rightarrow O_2^- \rightarrow O_4^- \rightarrow CO_4^- \rightarrow O_3^- \rightarrow CO_3^- \rightarrow NO_3^-$
162	$e \rightarrow O_2^- \rightarrow O_4^- \rightarrow CO_4^- \rightarrow O_3^- \rightarrow CO_3^- \rightarrow NO_2^- \rightarrow NO_3^-$
499	$e \rightarrow O_2^- \rightarrow O_3^- \rightarrow CO_3^-$
501	$e \rightarrow O_2^- \rightarrow CO_4^- \rightarrow CO_3^-$
503	$e \rightarrow O_2^- \rightarrow O_4^- \rightarrow O_3^- \rightarrow CO_3^-$
504	$e \rightarrow O_2^- \rightarrow CO_4^- \rightarrow O_3^- \rightarrow CO_3^-$
506	$e \rightarrow O_2^- \rightarrow O_4^- \rightarrow CO_4^- \rightarrow CO_3^-$
507	$e \rightarrow O_2^- \rightarrow O_4^- \rightarrow CO_4^- \rightarrow O_3^- \rightarrow CO_3^-$

less than 1% to the total transmittance leading to this ion. Understanding of the negative ion chemistry can be completed by showing the loss rates (s^{-1}) as in Figure 8. The extremely high loss rate of O^- explains why the ion is not even shown in Figure 4. The effect of the high production rate of O_2^- (see Figure 6) is easily attenuated by its high loss rate shown in Figure 8. Furthermore, the fact that NO_3^- is the major negative ion in the reference model, can now be understood since its loss rate in Figure 8 is extremely small. As a consequence, a weak production path can significantly contribute to the build-up of NO_3^- ions. As an example, path 77 (see Fig. 7 and Table 3) which only represents 9% of the NO_3^- production at 50 km, is the second production path (25%) above 60 km altitude. Furthermore, the O_4^- production by the reaction between O_2^- and O_2 is so small that it represents less than two percents of the total O_2^- loss at 65 km. A similar situation is found for path 68 which approximately accounts for 6% of the NO_3^- production at 65 km. The transitions from O_2^- to CO_4^- and from CO_4^- to NO_3^- both represent less than one percent of the total losses of O_2^- and CO_4^- respectively. Such a situation could lead to the omission of path 77 or 68 if signal flow graph technique had not been used, despite the fact that the cumulative production of this two paths represents approximately 30% of the NO_3^- production.

Finally, Figure 7 clearly indicates above 60 km that path 499 practically leads to the whole CO_3^- production and its extension (path 102) is responsible for the NO_3^- production for which the loss rate is very small. As it is pointed out in Appendix B, the relative losses along a specific path determine its absolute importance. Since atomic oxygen and nitric oxide influence the loss of CO_3^-, one can expect that variations of these neutral constituents play a role in the negative ion production. This aspect is discussed in section 5.

At lower heights, around 50 km, other paths become significant in addition to path 499. The most important reaction chains at

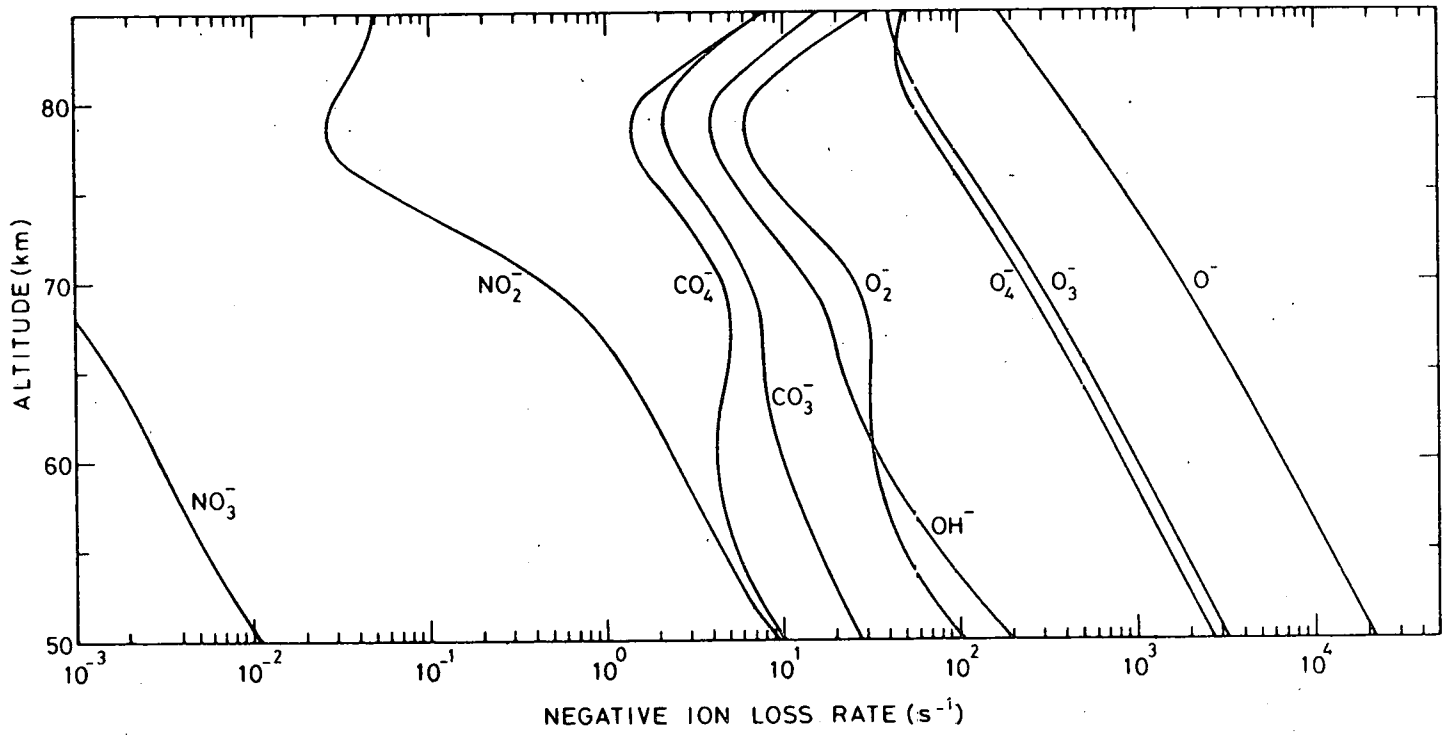

Fig. 8. Vertical profiles of some negative ion loss rates (s^{-1}) for the external input γ_e of Fig. 3.

50 km are shown in Figure 9 which gives also the major paths at 60 km. The appearance of this new paths at 50 km is essentially a consequence of the increase in the neutral concentration which favors the reaction $O_2^- + O_2 + M \rightarrow O_4^- + M$ with respect to the reaction $O_2^- + O_3 \rightarrow O_3^- + O_2$. The situation for CO_4^- at 50 km is similar to that one of CO_3^- at 60 km, since any increase in nitric oxide favors NO_3^- production. Furthermore, a decrease in ozone gives more importance to the paths going through CO_4^-. Finally the feedback reactions from O_2^- to e (see Figure 1) largely depend on the concentrations in atomic oxygen and excited molecular oxygen $O_2(^1\Delta_g)$.

In summary, Figures 5 to 8 computed for an input γ_e, indicate the type of analysis which can be made with the signal flow graph technique. Similar studies can be undertaken by considering reaction rates, photodetachment rates or neutral concentrations as variable parameters. Since we only used measured rate coefficients (Albritton, 1978; Ferguson, 1974; Smith et al. 1978; Smith et al. 1976; Truby, 1972; Phelps, 1969; Stelman et al. 1972; Mul and McGowan, 1979) we prefer to indicate in the following section the effect of variations in the neutral model which essentially results from theoretical computations (Keneshea et al. 1979; Turco and Sechrist, 1970, 1972b). It does not imply that the neutral models are unreliable, but variations of neutral minor constituents are real geophysical phenomena which can induce significant ionospheric modifications.

5. EFFECT OF VARIATIONS OF THE MINOR NEUTRAL CONSTITUENTS

It has been shown in the preceeding section how the height variation of the neutral atmosphere can affect the paths leading to NO_3^- and CO_3^- ions. Nitric oxide, atomic oxygen, ozone and excited molecular oxygen are of major importance in the evaluation of the transmittances associated to the predominant paths. It is, therefore, interesting to evaluate their effects at 65 km altitude where NO_3^- is the major negative

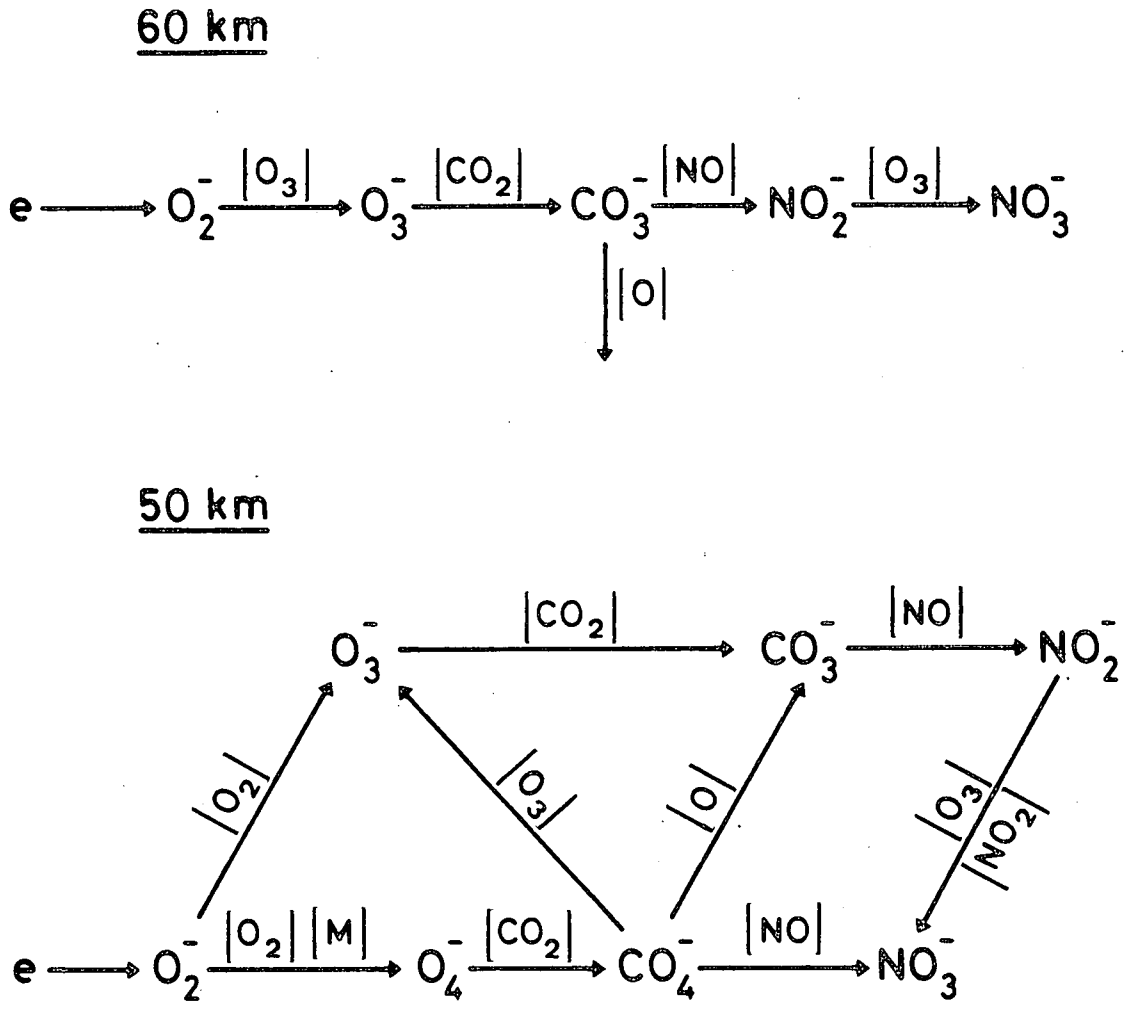

Fig. 9. Comparison of the reaction chains leading to NO_3^- at 60 km and 50 km altitude.

ion in the reference model. At 65 km altitude, the neutral model adopted in section 2 leads to the following concentrations : $n(NO) = 2.9 \times 10^8$ cm^{-3}, $n(O) = 3.5 \times 10^{10}$ cm^{-3}, $n(O_3) = 1.3 \times 10^{10}$ cm^{-3} and $n(O_2\ ^1\Delta_g) = 4.6 \times 10^{10}$ cm^{-3}.

In an analysis of minor constituents in the middle atmosphere, Ackerman (1979) indicates that nitric oxide measurements at 65 km range between 10^7 cm^3 and 2×10^8 cm^{-3}. We adopt here an arbitrary variation from 10^7 cm^{-3} to 10^9 cm^{-3}. When all other parameters of the reference model are kept constant, such a variation leads to the results shown in the left part of Figure 10. It appears that an increase of NO at 65 km altitude leads to an increase of NO_3^- accompanied by a decrease of CO_3^-, of HCO_3^- and of the electron concentration. The dimensionless ratio λ is also shown and the vertical arrow corresponds to the nitric oxide concentration in the reference model. It is important to note that a variation of NO can lead to a significant change of the rate λ between negative ions and electrons. It should be noted that variations of NO at 65 km do not significantly modify the input γ_e of Figure 3, since at this altitude the electron ion pair production essentially results from cosmic rays without Lyman-α production of NO^+.

A detailed analysis of the nitric oxide effect is presented in Table 4. This table gives the total transmittance T_t and the total loss L of NO_3^- as a function of the nitric oxide concentration. Path gains g_i, amplification factors Δ_i/Δ, partial transmittances T_i are given for several paths labelled i and shown in Table 3. The transmittances T_i are related by Eq. (8) to the production in Fig. 7. The lines labelled $\%_i$ give the importance of path i in percents. It appears that the importance of a path changes as a function of the nitric oxide concentration but not in the same way as the corresponding path gain. As an example, path 82 has a path gain g_{82} unaffected by nitric oxide variations. But its amplification factor Δ_{82}/Δ decreases slowly with an increase of nitric oxide, and the partial transmittance T_{82} decreases in

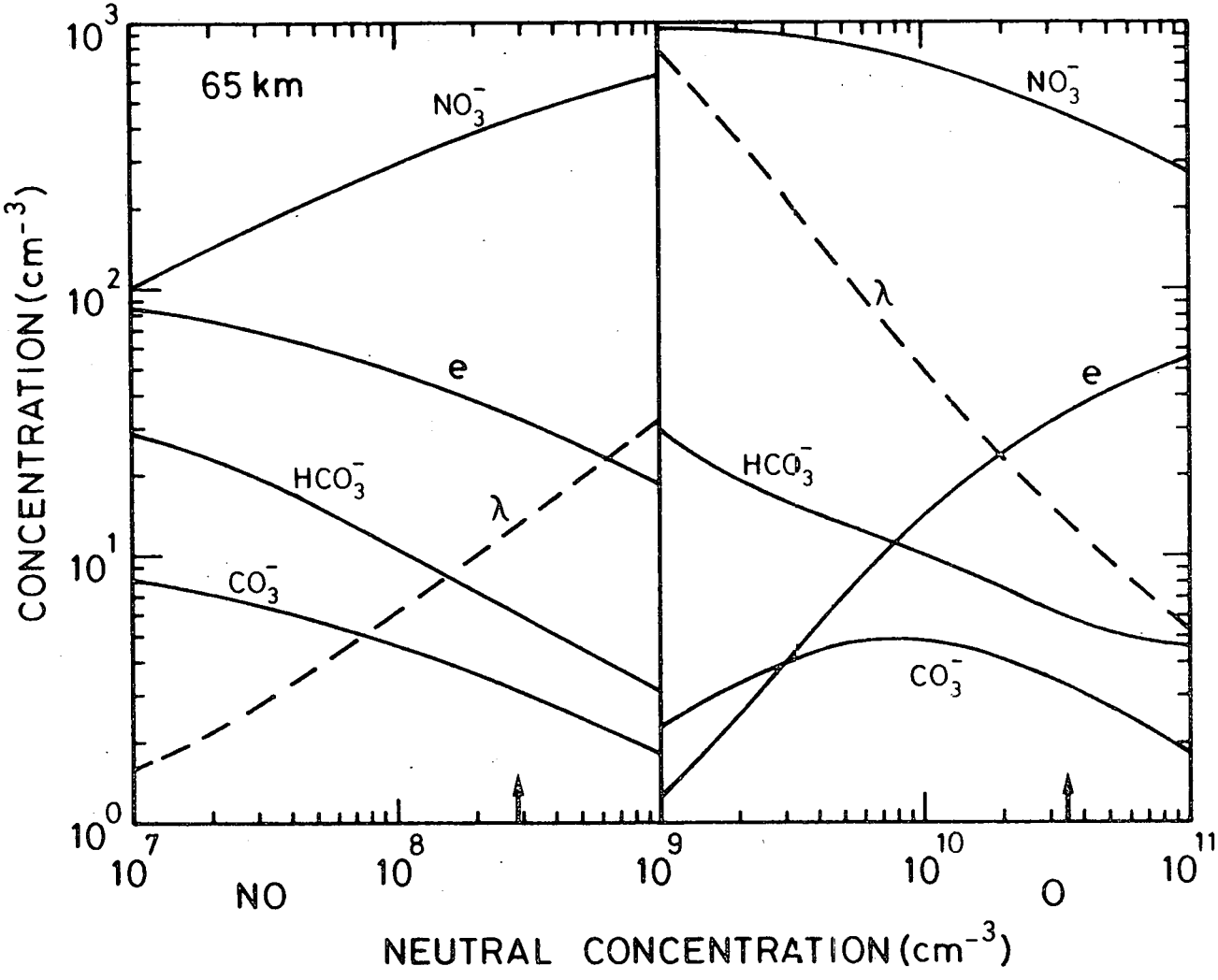

Fig. 10. Electron and negative ion concentrations at 65 km as a function of nitric oxide concentration (left part) and of atomic oxygen concentration (right part). The dimensionless ratio λ is also shown. The vertical arrows indicate the NO and O concentrations used in the reference model of Fig. 4.

Table 4 : Signal flow graph characteristics for NO_3^- as a function of nitric oxide concentration at 65 km altitude.

$n(NO)(cm^{-3})$	1×10^7	5×10^7	1×10^8	5×10^8
T_t	2.13	4.85	6.74	15.1
L	1.29×10^{-3}	1.34×10^{-3}	1.39×10^{-3}	1.80×10^{-3}
$\%_{77}$	17.4	21.2	21.6	22.3
g_{77}	2.09×10^{-6}	1.04×10^{-5}	2.10×10^{-5}	1.04×10^{-4}
Δ_{77}/Δ	1.78×10^5	9.87×10^4	7.05×10^4	3.24×10^4
T_{77}	0.372	1.03	1.48	3.38
$\%_{82}$	7.7	1.8	< 1.0	< 1.0
g_{82}	4.44×10^{-7}	4.42×10^{-7}	-	-
Δ_{82}/Δ	3.74×10^5	2.08×10^5	-	-
T_{82}	0.166	0.092	-	-
$\%_{102}$	48.5	59.3	60.9	62.4
g_{102}	2.78×10^{-6}	1.38×10^{-5}	2.78×10^{-5}	1.38×10^{-4}
Δ_{102}/Δ	3.74×10^5	2.08×10^5	1.48×10^5	6.82×10^4
T_{102}	1.04	2.88	4.11	9.43

the same way as Δ_{82}/Δ. The two other paths 77 and 102 have path gains which increase with nitric oxide. In this case the decrease of the amplification factors Δ_{77}/Δ and Δ_{102}/Δ is not sufficient to prevent an increase of the partial transmittances T_{77} and T_{102}. As a result, the importance of path 82 strongly decreases when nitric oxide increases and this path represents less than one percent of the total transmittance when the nitric oxide concentration reaches a value of 10^8 cm^{-3}.

A similar analysis made for CO_3^- indicates a decrease of the transmittance resulting from a decrease in the amplification factor of path 499 which always remains the most important path.

The righthand part of Figure 10 shows the effect of a variation in atomic oxygen. Since O, O_3 and $O_2(^1\Delta_g)$ are not independent quantities in the neutral chemistry, variations of atomic oxygen are assumed to be accompanied by ozone and excited molecular oxygen such that the ratios $n(O_3)/n(O)$ and $n(O_2\ ^1\Delta_g)/n(O_3)$ are identical to the values of the reference model as well as the nitric oxide concentration. Figure 10 shows that any increase in atomic oxygen produces an increase of the electron concentration and a subsequent decrease of the ratio λ. The concentrations of NO_3^- and HCO_3^- decrease when atomic oxygen increases. The maximum in CO_3^- concentration results from a competition between CO_3^- partial production and loss rates as a function of atomic oxygen. For atomic oxygen concentrations greater than 8×10^9 cm^{-3} the increase of CO_3^- production is smaller than the increase of CO_3^- loss by atomic oxygen.

6. CONCLUSION

In a study of D-region ion chemistry the quantitative effect of any parameter can be analyzed in detail by applying Mason's (1956) rules to the corresponding signal flow graph. With these rules it is

possible to evaluate quantitatively each production path and to know how each parameter influences the path gain or the amplification factor which is a measure of the chemical loops present in the system.

Negative ion clusters have been omitted in this paper but any new reaction or new rate coefficient can be introduced in a straightforward manner. The major objective here is to present a tool appropriate to the analysis of large chemical systems under steady state conditions without transport effects. Nevertheless, the example at 65 km altitude clearly indicates significant variations of the negative ion concentrations as a function of adopted nitric oxide and atomic oxygen concentrations.

APPENDIX A : SIGNAL FLOW GRAPH AND MASON'S RULES

A graph is a set of nodes and edges which join two distinct nodes. The nodes in Figure 1 are the various negative ions and the edges are the oriented lines joining the ions. A path is composed by successive edges which never pass through the same node. A loop is a path for which the first node is identical to the last node. When numerical values are given to each edge, the value for a certain path or loop is simply the product of the values of the edges composing the path or the loop. These values are sometimes called path gains or loop gains.

Let us consider a system of k linear equations given by

$$x_i = \sum_{\substack{j=1 \\ j \neq i}}^{k} c_{ij} x_j + d_i \qquad (A.1)$$

The flow graph associated with this system has the following characteristics : each unknown quantity x_i is associated to a node of the graph, each coefficient c_{ij} is the value of the edge oriented from j towards i and the terms d_i represents various external inputs to the system. The edge joining an input IN to a node has always a value equal to one.

The system (A.1) can be solved by classical methods. Such a procedure, however, gives no information on the relative importance of the various paths or loops in the associated graph. Mason (1956) developed a technique which expresses each unknown x_i of the system (A.1) as a function of the various inputs and a quantity called transmittance which depends on the values associated to the edges composing the graph. For m inputs IN corresponding to the values d_i in (A.1), each unknown x_i is given (Henley and Williams, 1973) by

$$x_i = \sum_{j=1}^{m} T_{(i \leftarrow j)} \; x \; (IN)_j \qquad (A.2)$$

where the transmittance $T_{(i \leftarrow j)}$ is

$$T_{(i \leftarrow j)} = \sum_{l=1}^{n} g_\ell \; \Delta_\ell / \Delta \quad , \qquad (A.3)$$

n being the number of paths joining the input $(IN)_j$ to the node i. In expression (A.3), g_ℓ is the numerical value (path gain) associated with each path joining the input j to the node i. The path gain g_ℓ is always a product of edge values c_{ij}. The quantities Δ and Δ_ℓ depend on the structure of the various loops in the graph. Δ is given by (Mason, 1956; Henley and Williams, 1973)

$$\Delta = 1 - \Sigma_1 + \Sigma_2 - \Sigma_3 + \ldots \qquad (A.4)$$

where Σ_1 is the sum of all loop gains in the graph, Σ_2 is the sum of products of all loop gains taken two at a time but excluding touching loops and Σ_3 is the sum of products of all loop gains taken three at a time but excluding touching loops. Δ_ℓ is obtained from Δ by deleting the loop gain terms touched by the ℓ-th path.

For a given input the transmittance is the product of g_ℓ by Δ_ℓ/Δ where g_ℓ is the path gain and Δ_ℓ/Δ is an factor resulting from all recycling loops existing in the graph. If there is no loop in the graph Δ_ℓ/Δ is equal to one.

APPENDIX B : SIGNAL FLOW GRAPH AND ION CHEMISTRY IN THE D REGION

When transport processes are neglected, the steady state concentrations of positive (or negative) ions in the D region are obtained by equating production and loss terms for each ion. Furthermore, the electroneutrality condition can be used in a way such that the system of equations is linear. Mason's rules described in Appendix A are, therefore, directly applicable. Instead of writing a system of equations like (A.1) in terms of concentrations it is more efficient to work with productions since, in this case, the path gains have a real geophysical significance as it will be shown in the present appendix.

For k negative ions including the electrons, the production rate P_i ($cm^{-3}\ s^{-1}$) of the i-type ion is given by

$$P_i = n_i\ L_i = \sum_{\substack{j=1 \\ j\neq i}}^{k} r_{ij}\ n_j + \gamma_i \qquad (B.1)$$

where L_i (s^{-1}) is the total loss rate of the i-type ion with concentration n_i and γ_i is an external production rate ($cm^{-3}\ s^{-1}$) which is zero for all negative ions and equal to γ_e for electrons. The coefficients r_{ij} can be considered as reaction rates in s^{-1} which depend on the various rate coefficients, the neutral concentrations and the positive ion concentrations.

System (B.1) can also be written as

$$P_i = n_i\ L_i = \sum_{\substack{j=1 \\ j\neq i}}^{k} r_{ij}\ (L_j\ n_j/L_j) + \gamma_i \qquad (B.2)$$

or

$$P_i = \sum_{\substack{j=1 \\ j \neq i}}^{k} (r_{ij}/L_j)\, P_j + \gamma_i \qquad (B.3)$$

where P_j and L_j are the production rate ($cm^{-3}\ s^{-1}$) and the total loss rate (s^{-1}) of the j- type ion, respectively. The system of equations (B.3) is formaly identical to the system (A.1) and Mason's rules (A.2), (A.3) and (A.4) can be used to obtain the productions P_i in terms of inputs and transmittances. Knowing each production P_i, the individual concentrations n_i are obtained from $n_i = P_i/L_i$. Up to this point the signal flow graph gives exactly the same information as a classical solution, but the application of Mason's rules gives also the various transmittances indicating which physical process is important and how an input to the system is transferred to an ion through a specific path. Such an advantage is particularly rewarding when a large number of reactions are involved. Finally the adoption of the productions P_i as unknowns leads to a simple interpretation of the terms r_{ij}/L_j which can be considered as relative loss rates. The coefficient r_{ij} is the loss rate of the j- type ion towards i- type ions and L_j is the total loss rate of the j- type ion.

Although a detailed proof is not simple, it has been shown (Henley and Williams, 1973) that Mason's rules lead to solutions of the system (A.1) identical to result obtained from other methods. For the comprehension of the signal flow graph technique we consider an over-simplified scheme of reactions involving only electrons and O_2^- ions as given in Table B1. When Mason's rules are applied to the corresponding system (B.3) it is usefull to check two points : (1) the solution obtained with Mason's rules is identical to the classical algebraic solution of system (B.3); (2) the solution obtained with Mason's rules is

Table B1 : Reactions used in an oversimplified e-O_2^- system.

M + photon or particle	→	$e + M^+$	$\gamma_e (cm^{-3}s^{-1})$
$e + M^+$	→	neutrals	$\alpha_1 (cm^3 s^{-1})$
$e + O_2 + M$	→	$O_2^- + M$	$k_1 (cm^6 s^{-1})$
$e + O_2$	→	O_2^-	$k_2 (cm^3 s^{-1})$
$O_2^- + O$	→	$e + O_3$	$k_3 (cm^3 s^{-1})$
$O_2^- + O_2(^1\Delta_g)$	→	$e + 2O_2$	$k_4 (cm^3 s^{-1})$
O_2^- + photon	→	$e + O_2$	$J_1 (s^{-1})$
$O_2^- + M^+$	→	neutrals	$\alpha_2 (cm^3 s^{-1})$

identical to the solution obtained by equating electron or O_2^- production rates to their corresponding loss rates.

The signal flow graph is shown in Figure B1 where several transitions from O_2^- to e and from e to O_2^- are represented by one edge respectively. This procedure is not mandatory but it decreases significantly to total number of paths which have to be memorized in the graph analysis. The system (B.3) reduces to

$$P_e = (r_{e,\,O_2^-}/L_{O_2^-})\, P_{O_2^-} + \gamma_e \qquad (B.4)$$

and

$$P_{O_2^-} = (r_{O_2^-,\,e}/L_e)\, P_e \qquad (B.5)$$

The algebraic solutions of this system are

$$P_e = \gamma_e/[1 - (r_{e,O_2^-}/L_{O_2^-})\,(r_{O_2^-,e}/L_e)] \qquad (B.6)$$

and

$$P_{O_2^-} = \gamma_e\,(r_{O_2^-,e}/L_e)/[1 - (r_{e,O_2^-}/L_{O_2^-})\,(r_{O_2^-,e}/L_e)] \qquad (B.7)$$

According to Mason's rule (A.2) and noting only one input IN = γ_e in Figure B.1, one obtains with m = 1

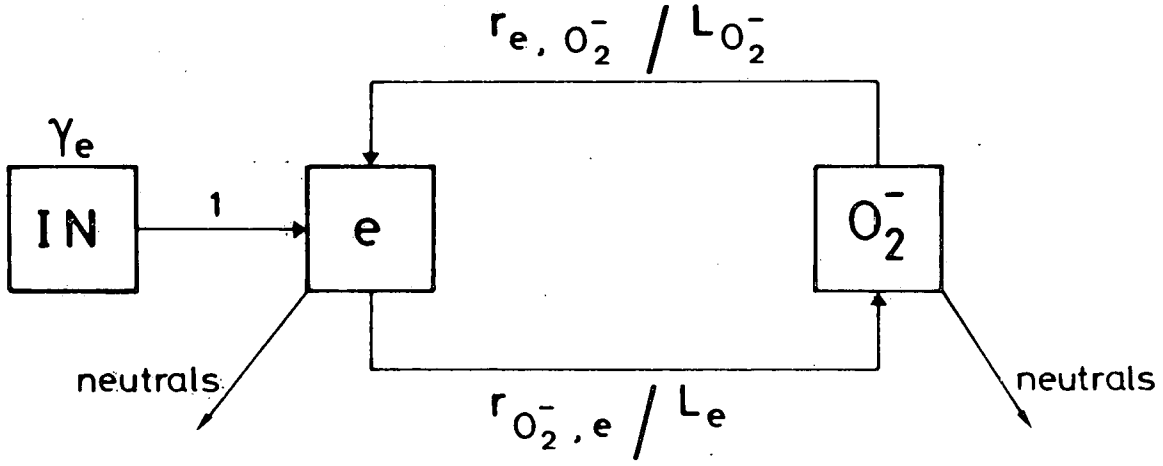

Fig. B1. Signal flow graph corresponding to the reactions of Table B1. All electron loss processes leading to O_2^- are combined under a single edge from e to O_2^-. The edge from O_2^- to e represents the three O_2^- loss processes of Table B1 giving rise to electrons. The input to the system is characterized by a production rate γ_e ($cm^{-3}s^{-1}$) and the path values are indicated on edge. Note that the value of the input edge is one.

$$P_e = T_{(e \leftarrow 1)} \times \gamma_e \qquad (B.8)$$

and

$$P_{O_2^-} = T_{(O_2^- \leftarrow 1)} \times \gamma_e \qquad (B.9)$$

Since there is only one path joining the input γ_e to the node e or O_2^-, the transmittances $T_{(e \leftarrow 1)}$ and $T_{(O_2^- \leftarrow 1)}$ are given from (A.3) as

$$T_{(e \leftarrow 1)} = g_1 \Delta_1/\Delta \qquad (B.10)$$

$$T_{(O_2^- \leftarrow 1)} = g_1' \Delta_1'/\Delta \qquad (B.11)$$

For the electrons the path gain is $g_1 = 1$ along the path IN → e and for O_2^-, the path gain is $g_1' = 1 \times (r_{O_2^-,c}/L_c)$ along the path IN → e → O_2^-. Since the graph in Figure B.1 only contains one loop, Equation (A.4) leads to

$$\Delta = 1 - \Sigma_1 = 1 - (r_{e,\ O_2^-}/L_{O_2^-})\ (r_{O_2^-,e}/L_e) \qquad (B.12)$$

Since this sole loop touches the path IN → e and the path IN → e → O_2^-, one has $\Delta_1 = \Delta_1' = 1$. The transmittances (B10) and (B11) can finally be written as

$$T_{(e \leftarrow 1)} = 1/[1 - (r_{e,O_2^-}/L_{O_2^-})\ (r_{O_2^-,e}/L_e)] \qquad (B.13)$$

and

$$T_{(O_2^- \leftarrow 1)} = (r_{O_2^-,e}/L_e)/[1 - (r_{e,O_2^-}/L_{O_2^-})\ (r_{O_2^-,e}/L_e)] \qquad (B.14)$$

which lead with (B8) and (B9) to production rates identical to Equations (B6) and (B7). Denoting a concentration by the corresponding chemical symbol in brackets, it can be seen from Table B1 that

$$L_e = k_1\ [O_2]\ [M] + k_2\ [O_2] + \alpha_1\ [M^+] \qquad (B.15)$$

$$r_{O^-,e} = k_1\ [O_2]\ [M] + k_2\ [O_2] \qquad (B.16)$$

$$L_{O^-} = k_3\ [O] + k_4\ [O_2(^1\Delta_g)] + J_1 + \alpha_2\ [M^+] \qquad (B.17)$$

and

$$r_{e,O^-} = k_3\ [O] + k_4\ [O_2(^1\Delta_g)] + J_1 \qquad (B.18)$$

where L_e and $L_{O_2^-}$ are the total loss rates in s^{-1} for electrons and O_2^- ions, respectively; $r_{O_2^-,e}$ is the partial loss rate of electrons which are converted in O_2^- and r_{e,O_2^-} is the partial loss rate of O_2^- ions which lead to electrons. The relative loss rates r_{ij}/L_j play the fundamental role in the transmittances. Substitution of Equations (B15) to (B18) in the transmittances leads to production rates P_e and $P_{O_2^-}$ which, if divided by L_e and $L_{O_2^-}$, respectively, give electron and O_2^- concentrations identical to the classical result obtained without graph analysis.

The fundamental advantage of the application of Mason's rule is the access to the various transmittances which give a physical insight how a complicated system depends on some specific reactions. The term g_ℓ in the transmittance gives the path gain towards a specific constituent when a path ℓ is followed from the input. In other word g_ℓ measures the capacity of a specific path to transmit an external production. The term Δ_ℓ/Δ is an amplification factor resulting from recycling processes. This factor measures the feedback mechanisms in the chemical system.

ACKNOWLEDGMENTS

We are grateful to S.P. Zimmerman, T.J. Keneshea and C.R. Philbrick for sending us numerical values for the neutral atmosphere model. The constructive comments of the anonymous referees are also appreciated.

REFERENCES

ACKERMAN, M., In situ measurements of middle atmosphere composition, J. Atmos. Terr. Phys., 41, 723-733, 1979.

ALBRITTON, D.L., Ion-neutral reaction-rate constants measured in flow reactors through 1977, Atom. Data Nucl. Data Tables, 22, 1-101, 1978.

ARIJS, E., J. INGELS, and D. NEVEJANS, Mass spectrometric measurement of the positive ion composition in the stratosphere, Nature, 271, 642-644, 1978.

ARNOLD, F., H. BÖHRINGER, and G. HENSCHEN, Composition measurements of stratospheric positive ions, Geophys. Res. Lett., 5, 653-656, 1978.

ARNOLD, F., and G. HENSCHEN, First mass analysis of stratospheric negative ions, Nature, 275, 521-522, 1978.

ARNOLD, F., J. KISSEL, D. KRANKOWSKY, H. WIEDER, and J. ZÄHRINGER, Negative ions in the lower ionosphere : a mass-spectrometer measurement, J. Atmos. Terr. Phys., 33, 1167-1175, 1971.

COSBY, P.C., J.H. LING, J.R. PETERSON, and J.T. MOSELEY, Photodissociation and photodetachment of molecular negative ions. III. Ions-formed in $CO_2/O_2/H_2O$ mixtures, J. Chem. Phys., 65, 5267-5274, 1976.

FERGUSON, E.E., Laboratory measurements of ionospheric ion-molecule reaction rates, Rev. Geophys. Space Phys., 12, 703-713, 1974.

FERGUSON, E.E., D.B. DUNKIN, and F.C. FEHSENFELD, Reaction of NO_2^- and NO_3^- with HCl and HBr, J. Chem. Phys., 57, 1459-1463, 1972.

GOLDBERG, R.A., and A.C. AIKIN, Studies of positive ion composition in the equatorial D-region ionosphere, J. Geophys. Res., 76, 8352-8364, 1971.

GOLDBERG, R.A., and L.J. BLUMLE, Positive ion composition from a rocket-borne mass spectrometer, J. Geophys. Res., 75, 133-142, 1970.

HENLEY, E.J., and R.A. WILLIAMS, Graph theory in modern engineering, Mathematics in Science and Engineering, Vol. 98, Academic Press, New York, 1973.

HUANG, C.-M., M. WHITAKER, M.A. BIONDI and R. JOHNSEN, Electron-temperature dependence of recombination of electrons with $H_3O^+ (H_2O)_n$ - series ions, Phys. Rev. A, 18, 64-67, 1978.

JOHANNESSEN, A., and D. KRANKOWSKY, Positive-ion composition measurement in the upper mesosphere and lower thermosphere at high latitude during summer, J. Geophys. Res., 77, 2888-2901, 1972.

KEESEE, R.G., N. LEE, and A.W. CASTLEMAN, Jr., Atmospheric negative ion hydration derived from laboratory results and comparison to rocket-borne measurements in the lower ionosphere, J. Geophys. Res., 84, 3719-3722, 1979.

KENESHEA, T.J., S.P. ZIMMERMAN, and C.R. PHILBRICK, A dynamic model of the mesosphere and lower thermosphere, Planet. Space Sci., 27, 385-401, 1979.

LEE, L.C., and G.P. SMITH, Photodissociation and photodetachment of moleculer negative ions. III. Ions in $O_2/CH_4/H_2O$ mixtures from 3500 to 8600 A, J. Chem. Phys., 70, 1727-1735, 1979.

MASON, S.J., Feedback theory - Further properties of signal flow graphs, Proc. IRE, 44, 920-926, 1956.

MUL, P.M., and J. Wm. McGOWAN, Merged electron-ion beam experiments III. Temperature dependence of dissociative recombination for atmospheric ions NO^+, O_2^+, and N_2^+, J. Phys. B, Atomic Molec. Phys., 1591-1601, 1979.

NARCISI, R.S., Ion composition of the mesosphere, Space Res., 7, 186-196, 1967.

NARCISI, R.S., and A.D. BAILEY, Mass spectrometric measurements of positive ions at altitudes from 64 to 112 kilometers, J. Geophys. Res., 70, 3687-3700, 1965.

NARCISI, R.S., A.D. BAILEY, L. DELLA LUCA, C. SHERMAN, and D.M. THOMAS, Mass spectrometric measurements of negative ions in the D- and lower E- regions, J. Atmos. Terr. Phys., 33, 1147-1159, 1971.

NARCISI, R.S., A.D. BAILEY, L.E. WLODYKA, and C.R. PHILBRICK, Ion composition measurements in the lower ionosphere during the November 1966 and March 1970 solar eclipses, J. Atmos. Terr. Phys., 34, 647-658, 1972.

PHELPS, A.V., Laboratory studies of electron attachment and detachment processes of aeronomic interest, Canad. J. Chem., 47, 1783-1793, 1969.

REID, G.C., Physical processes in the D region of the ionosphere, Rev. Geophys., 2, 311-333, 1964.

REID, G.C., Ion chemistry in the D region, in Advances in Atomic and Molecular Physics, vol. 12, edited by D.R. Bates and B. Bederson, pp. 375-413, 1976.

SMITH, D., N.G. ADAMS, and M.J. CHURCH, Mutual neutralization rates of ionospherically important ions, Planet. Space Sci., 24, 697-703, 1976.

SMITH, E.V.P., and D.M. GOTTLIEB, Solar flux and its variations, Space Sci. Rev., 16, 771-802, 1974.

SMITH, G.P., and L.C. LEE, Photodissociation of atmospheric positive ions. II. 3500-8600 A, J. Chem. Phys., 69, 5393-5399, 1978.

SMITH, G.P., L.C. LEE, P.C. COSBY, J.R. PETERSON, and J.T. MOSELEY, Photodissociation and photodetachment of molecular negative ions. V. Atmospheric ions from 7000 to 8400 A, J. Chem. Phys., 68, 3818-3822, 1978.

STELMAN, D., J.L. MORUZZI, and A.V. PHELPS, Low energy electron attachment to ozone using swarm techniques, J. Chem. Phys., 56, 4183-4189, 1972.

SWIDER, W., Aeronomic aspects of the polar D-region, Space Sci. Rev., 20, 69-114, 1977.

THOMAS, L., Recent developments and outstanding problems in the theory of the D region, Radio Sci., 9, 121-136, 1974.

THOMAS, L., P.M. GONDHALEKAR, and M.R. BOWMAN, The influence of negative-ion changes in the D- region during sudden ionospheric disturbances, J. Atmos. Terr. Phys., 35, 385-395, 1973a.

THOMAS, L., P.M. GONDHALEKAR, and M.R. BOWMAN, The negative-ion composition of the daytime D-region, J. Atmos. Terr. Phys., 35, 397-404, 1973b.

TRUBY, F.K., Low-temperature measurements of the three-body electron-attachment coefficient in O_2, Phys. Rev. A, 6, 671-676, 1972.

TURCO, R.P., A discussion of possible negative ion detachment mechanisms in the sunrise D region, Radio Sci., 9, 655-658, 1974.

TURCO, R.P., and C.F. SECHRIST, Jr., An investigation of the ionospheric D region at sunrise, Aeron. Rep. 41, Aeron. Lab. Univ. Ill. Urbana-Champaign, 1970.

TURCO, R.P., and C.F. SECHRIST, Jr., An investigation of the ionospheric D region at sunrise, 2, Estimation of some photo-detachment rates, Radio Sci., 7, 717-723, 1972a.

TURCO, R.P., and C.F. SECHRIST, Jr., An investigation of the ionospheric D region at sunrise, 3, Time variations of negative-ion and electron densities, Radio Sci., 7, 725-737, 1972b.

U.S.STANDARD ATMOSPHERE, 1976, U.S. Government Printing Office, Washington, D.C. 20402, 1976.

ZBINDEN, P.A., M.A. HIDALGO, P. EBERHARDT, and J. GEISS, Positive ion composition in the lower ionosphere during the Geminid meteor shower and the occurence of a winter anomaly, in Methods of Measurements and Results of Lower Ionosphere Structure, edited by K. Rawer, pp. 281-286, Akademie-Verlag, Berlin, 1974.

ZBINDEN, P.A., M.A. HIDALGO, P. EBERHARDT, and J. GEISS, Mass spectrometer measurements of the positive ion composition in the D- and E- regions of the ionosphere, Planet. Space Sci., 1621-1642, 1975.